IV International Conference on Particle-based Methods – Fundamentals and Applications
PARTICLES 2015
E. Oñate, M. Bischoff, D.R.J. Owen, P. Wriggers & T. Zohdi (Eds)

MODELING OF ELASTO-PLASTIC BEHAVIOUR OF GRANULAR MATERIALS USING MULTI-PARTICLE FINITE ELEMENT SIMULATIONS

Nouha ABDELMOULA[1]*, Barthélémy HARTHONG[1], Didier IMBAULT[1] and Pierre DORÉMUS[1]

[1] Université Joseph Fourier/INPG/CNRS, UMR 5521 3SR
Domaine Universitaire, BP 53, 38041 Grenoble cedex 9, France
*abdelmoula.noouha@gmail.com

Key words: Granular Materials, Multi-Particles Finite Element Method, Yield Surface, Flow Rule, Elasto-plasticity, Multi-scale Modelling

Abstract. The method of multi-particle finite element involving assemblies of meshed particles interacting through finite-element contact conditions is adopted to study the plastic flow of a granular material with highly deformable elastic-plastic grains. In particular, it is investigated whether the flow rule postulate applies for such materials. Using a spherical stress probing method, the influence of incremental stress on plastic strain increment vectors was assessed for numerical samples compacted along two different loading paths up to different values of relative density. Results show that the numerical samples studied behave reasonnably well according to an associated flow rule, except in the vicinity of the loading point where the influence of the stress increment proves to be very significant. The influence of relative density and initial loading path is discussed.

1 INTRODUCTION

Powder metallurgy includes several processes for the shaping of ductile metal powder. Among these, cold compaction of powders followed by sintering is one of the most commonly used in the industry, allowing the manufacturing of complex shaped engineering components and substantial cost savings. This paper is concerned with the cold compaction stage. During this step, powders undergo large deformation accompanied by a significant densification. For instance, the initial volume after die filling for iron powder (initial density is about $3.3g/cm^3$) is reduced by about half (final density is about $7.1g/cm^3$) at the end of the compaction step [1].

During compaction, failure can occur as a result of a locally highly deviatoric loading close to singularities of complex-shaped parts. This failure mechanism is poorly understood, such that manufacturers currently undertake long and costly trials and errors campaigns to obtain defectless parts. There is a need for numerical modelling of the cold

compaction process involving reliable failure criteria for powder materials. But before getting a failure criterion it is necessary to have a constitutive model for powders so as to reproduce the evolution of stresses and strains throughout compaction.

Currently available models are variants of the Drucker-Prager Cap model [2] that is available in commercial finite-element codes, and has been proved to be reliable in the average sense. But Drucker-Prager Cap model is based on persistent isotropy, which has been proved to be clearly wrong for powder materials by several experimental studies involving triaxial experiments, such as [3]. Yet, taking compaction-induced anisotropy into account is necessary to correctly reproduce the evolution of stresses and strains for singular loading paths, precisely where failure might occur.

The Drucker-Prager Cap model [2] and its variants are based on so-called classical elasto-plasticity, i.e., on the concepts of yield surface and flow rule based on plastic potential. Experimental studies such as [1, 3, 4] have given enough data to model the shape of yield surfaces, but very few of them [4] have given insight about plastic potential, which requires to separate incremental plastic strain and elastic strain.

To obtain more data about plastic deformation mechansims in powder materials, the Discrete Element Method (DEM) was introduced for the modeling of granular media in the fields of geomechanics and granular flow, and were then applied to hard and ductile powder materials [5, 6]. But this approach is not appropriate to describe grain deformations and use simplified contact formulations that become highly questionable for ductile particles when the relative density reaches a significant value [7], because deformable particles undergo a drastic change in shape.

Following [8, 9, 10], the present work uses the Multi-Particle Finite Element Method (MPFEM) which is based on finite element simulations of the mechanical behaviour of an assembly of meshed particles in contact. The use of finite element discretization and continuum mechanics modelling at particle scale in MPFEM combines discrete behavior of granular materials with the ability to accurately reproduce large contact deformation so as to simulate compaction from low (0.5) to high relative densities (0.98). This method is limited by its computational cost related to the large number of degrees of freedom required to simulate a relatively small number of particles. Despites this limitation, recent studies [11, 12] have proved the power of this method. The present paper applies MPFEM to the study of incremental plastic flow in powder materials.

2 METHOD

2.1 Numerical model

MPFEM simulations of the compaction of an assembly of particles under quasi-static loading conditions were carried out using an explicit integration scheme (commercial finite element program ABAQUS/Explicit). The use of this resolution scheme is adopted due to its capability to solve problems involving complex contact configurations and nonlinear constitutive behaviour including large strains kinematics. In this study, a polydisperse

assembly of 50 spherical particles was used (Fig. 1). The assembly was obtained using an algorithm accompanying open source DEM code YADE [13], consisting in generating 50 randomly disposed particles in a 1x1x1 (mm) cubic cell and growing their radii. When the particles start to touch each other, contact forces are created with respect to classical DEM algorithms. Particles rearrange and the procedure is stopped when stresses on the cell walls stabilise.

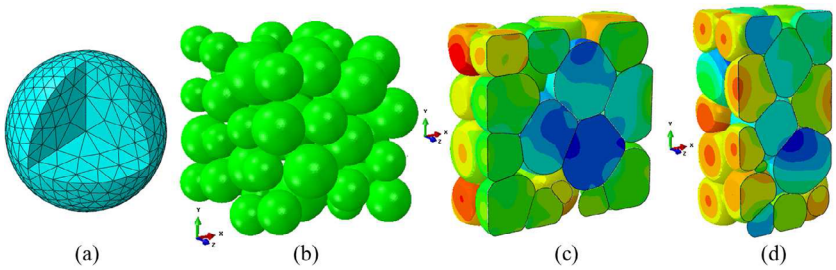

Figure 1: (a) Mesh for one particle. (b) Assembly of 50 undeformed particles. A section along the z plane: (c) after isotropic straining and (d) after closed die compaction by the MPFEM.

The model is then built in ABAQUS in the form of 50 meshed spherical particles surrounded by six rigid planes forming a cubic box of 1x1x1 (mm). Particles were meshed using approximately 3300 quadratic tetrahedral elements per particle. The mesh is made up of small elements at the boundary of the particle and larger elements in the center of the particle (Fig. 1.a). This configuration allowed optimising simulation time while maintaining a reasonable accuracy in the description of contact surfaces.

individual particles were assigned a constitutive model associating linear, isotropic elasticity (with elastic modulus E = 10 GPa and Poisson coefficient $\nu = 0.435$) and Mises plasticity with an isotropic power-law strain-hardening:

$$\sigma = k(\varepsilon^{pl})^n \tag{1}$$

Where $k = 20.5$ MPa and $n = 0.24$ are material parameters, and σ and ε^{pl} are, respectively, the Mises stress and the equivalent plastic strain. These parametres were calibrated on a lead alloy corresponding to the experimental tests performed by [10]. Particle/particle and particle/plane contact interactions were modeled by means of a penalty contact algorithm and a classical Coulomb friction law with a friction coefficient $f = 0.1$. No contact cohesion was introduced.

In the present study, the numerical assembly was compacted using either isotropic straining (referred to as isotropic compaction, Fig. 1.c) and uniaxial straining along x direction (referred to as closed die compaction, Fig. 1.d). Table 1 shows the order of magnitude of calculation time required for the two loading paths and three assemblies involving a different number of particles, up to a relative density $D = 0.9$. All simulations were run using parallel computing on with four Intel Xeon E7450 CPUs with 2.4 GHz using domain-level parallelisation.

Table 1: Calculation time using parallel computing with 4 CPUs

Samples	Loading paths	Calculation time
9 particles	Isotropic	6 hours
	Closed die	9 hours
15 particles	Isotropic	10 hours
	Closed die	12 hours
50 particles	Isotropic	19 hours
	Closed die	22 hours

Closed die compaction required more time than isotropic compaction due to larger displacements involved.

An important feature of the present work is that the numerical sample was limited to 50 particles to improve computational efficiency. An assembly of 50 particles is not sufficient to obtain a good representativeness of real powder materials in terms of averaged response. But it provides a large amount of qualitative but relevant information on the incremental plastic deformation mechanisms in real materials.

2.2 Probing of yield surfaces

In the present work, the numerical sample is compacted by means of the six rigid planes translating along their normal, so that initially parallel planes remain parallel throughout the loading. As a result, distortional strains are all kept to zero. Boundary conditions are either stress-driven (the total normal force on each plane is controlled to reach desired stress values) or strain-driven (normal displacements are imposed so that desired elongational strains are controlled). Using such boundary conditions, it can be checked that tangent force components on the rigid planes are negligible compared to normal components, meaning that no stress or strain rotation is applied. As a result, the numerical sample being initially isotropic, stress and strain principal directions are assumed to remain coaxial throughout the simulation. The consequence of such an approach is that the behaviour of the sample is only observed in the 3D principal stress space instead of the general 6D stress space.

Yield surfaces of the numerical sample were obtained as follows:

Step 1 The sample is compacted with a defined loading path (closed die compaction or isotropic compaction) up to a defined value of relative density D (Fig. 2.a). This step involves large deformations.

Step 2 The deformed sample is elastically unloaded to low (compressive) stress values to avoid any loss of contact between the planes and the sample (Fig. 2.b).

Step 3 The sample is reloaded with a proportional loading path in a defined direction of the stress space until the onset of plasticity is detected (Fig. 2.c).

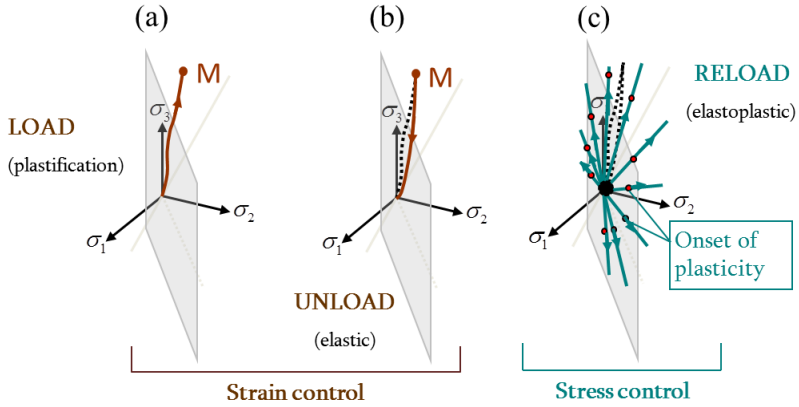

Figure 2: Method for probing yield surfaces: (a) First loading (Step 1), (b) unloading (Step 2), (c) reloading in various directions (Step 3).

For each reloading path (Step 3), this procedure gives one point of the yield surface of the sample corresponding to the strain-hardening state resulting from the initial loading (Step 1). To get the yield surface, Step 3 is repeated with a different loading direction, restarting simulations from Step 2. In the present study, the probing of yield surfaces is limited to the Rendulic plane of equation $\sigma_2 = \sigma_3$.

Step 1 is strain-driven so that rigid body motion of particles in the early rearrangement stage does not lead to huge displacement values for small applied stresses. Spherical stress probing simulations need to be conducted using stress control in the subsequent steps, as will be explained further. Transition from strain control to stress control is made between Step 2 and Step 3 so that small stress variations that might occur remain within the elastic range.

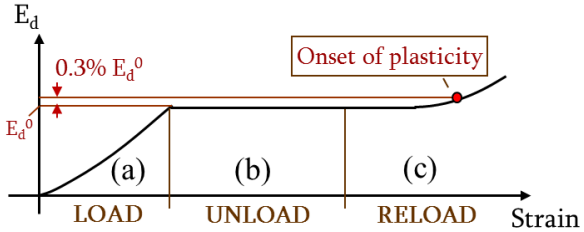

Figure 3: Determination of the onset of plasticity during (a) first loading, (b) unloading, and (c) reloading

Following [11], the detection of yield points during Step 3 is based on the total dissipation E_d, equal to the sum of plastic and frictional dissipation within the numerical model.

The onset of plasticity is defined as the point where the total dissipation in the assembly reaches a threshold value equal to $E_d^0 + 0.3\% E_d^0$, E_d^0 being the value of the total dissipation at the end of Step 1. Fig. 3 illustrates the evolution of the total dissipation between Step 1 and Step 3. Upon unloading, the total dissipation remains constant within a very good approximation (Fig. 3.b).

Fig. 4 shows the yield surfaces in a deviatoric stress/mean stress diagram with various values of final relative density D for the same assembly (50 particles) that was submitted to isotropic and closed die compaction. The results were qualitatively similar to known experimental [3] and numerical [12] results. As pointed out by [12], the evolution of yield surfaces on a monotonic loading path such as isotropic and closed die compaction was an approximately homothetic growth. Also, yield surfaces were oriented in the direction of the loading paths, which differed from the hydrostatic axis in the case of closed die compaction (Fig. 4.b) as a result of compaction-induced anisotropy.

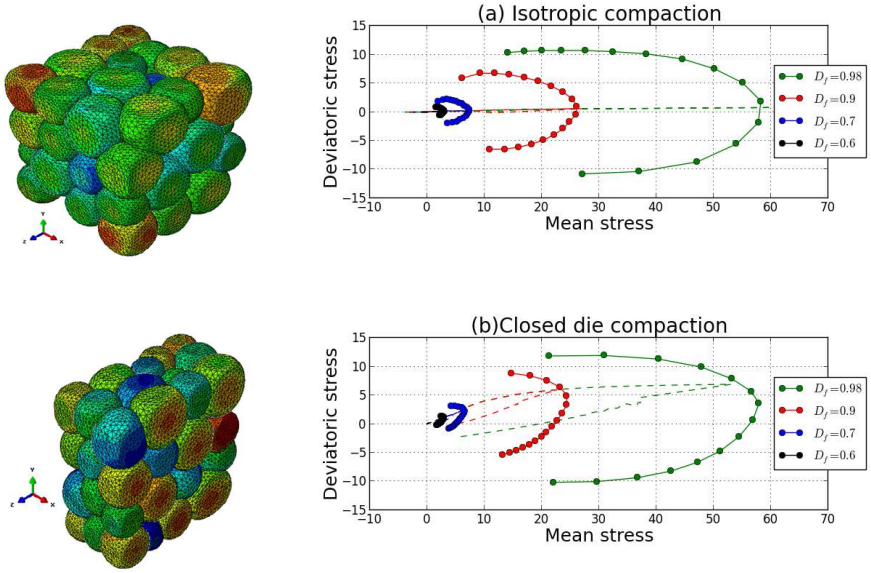

Figure 4: Evolution of yield surfaces from initial to various final relative density values, $D = 0.6$, 0.7, 0.9 and 0.98, with a monotonic loading: (a) isotropic compaction and (b) closed die compaction. The dotted line is the initial loading/unloading path.

2.3 Spherical stress probing method

In classical elasto-plasticity, the incremental plastic strain obeys the flow rule equation:

$$d\boldsymbol{\varepsilon}_{ij}^{pl} = \lambda \frac{\partial g\left(\boldsymbol{\sigma}, \chi\right)}{\partial \boldsymbol{\sigma}_{ij}} \tag{2}$$

where $d\boldsymbol{\varepsilon}^{pl}$ is the increment of plastic strain, $\boldsymbol{\sigma}$ the stress tensor, χ the strain-hardening variables, g the plastic potential and λ the plastic multiplier. Assuming g is regular,

equation (2) states that for a given state of stress and strain-hardening, the direction of the incremental plastic strain $d\boldsymbol{\varepsilon}^{pl}$ is unique.

In the present work, the existence of a plastic potential, and more generally, the incremental plastic flow could be studied on the numerical sample by using a spherical stress probing method [14, 15]. This method first consists in loading the numerical sample to a given state of stress $\boldsymbol{\sigma}_0$ on the yield surface (i.e. at the elastic limit, this corresponds to Step 3 as previously stated). Then, the two following steps are applied (Fig. 5):

Step 4 A small stress increment of magnitude $\Delta\sigma$ in a given direction is applied.

Step 5 The sample is unloaded back to $\boldsymbol{\sigma}_0$.

Assuming that no plastic dissipation occurs during the unloading phase conducted in Step 5, the incremental plastic strain $d\boldsymbol{\varepsilon}^{pl}$ was defined as the difference in total strain between the end of Step 3 and the end of Step 5.

Repeating Step 4 and Step 5 for different directions of the stress increment gives the incremental plastic strain vectors corresponding to the response of the sample to different stress increments $\Delta\sigma$ of same magnitude but different directions. The response of the sample were represented by the plastic strain response envelope, which is a closed surface containing the tips of all the plastic strain response vectors (such a surface for the stress increments would be a sphere). In the present paper, only stress increments in the Rendulic plane were applied.

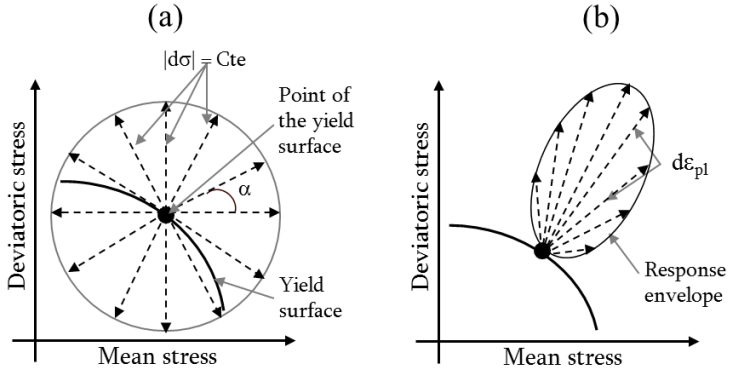

Figure 5: Method for detect the potential: (a) stress probes and (b) plastic strain response

Referring back to equation (2), if the flow rule applies and if a potential function exists, the plastic strain increment $d\boldsymbol{\varepsilon}^{pl}$ does not depend on the direction of $d\boldsymbol{\sigma}$. In such a case, the plastic strain response envelope is a line segment (Fig. 6.a), since the direction of $d\boldsymbol{\varepsilon}^{pl}$ is unique and entirely defined by $\boldsymbol{\sigma}$ and χ. If the response envelope of the plastic strain is not a straight line, then $d\boldsymbol{\epsilon}^{pl}$ depends on the direction of $d\boldsymbol{\sigma}$, which means that the flow rule equation (2) is not valid (Fig. 6.b).

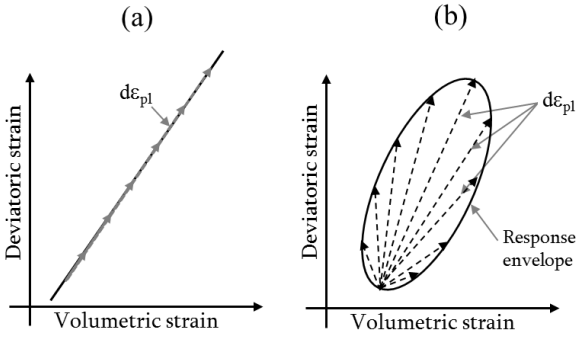

Figure 6: Plastic strain response envelope: (a) according to the flow rule postulate, (b) if the flow rule postulate is not valid.

3 RESULTS

In this section, plastic strain response envelopes are plotted in deviatoric strain/volumetric strain graphs in arbitrary units and superimposed to deviatoric stress/mean stress graphs with respect to the yield point they are associated to.

In order to preserve the aspect ratio of yield surfaces and plastic strain response envelopes, so as to visually assess normality of the flow rule, invariants of stress and strain were defined in a slightly unconventional way:

$$\begin{aligned} \sigma_M &= \tfrac{1}{\sqrt{3}}\left(\sigma_1+\sigma_2+\sigma_3\right); \quad \sigma_D = \sqrt{2/3}\left[\sigma_1 - \tfrac{1}{2}(\sigma_2+\sigma_3)\right]; \\ \varepsilon_V &= \tfrac{1}{\sqrt{3}}\left(\varepsilon_1+\varepsilon_2+\varepsilon_3\right); \quad \varepsilon_D = \sqrt{2/3}\left[\varepsilon_1 - \tfrac{1}{2}(\varepsilon_2+\varepsilon_3)\right]; \end{aligned} \tag{3}$$

where σ_M, σ_D, ε_M, ε_D are the mean stress, deviatoric stress, volumetric strain and deviatoric strain, respectively; σ_1, σ_2, σ_3, ε_1, ε_2, ε_3 are principal Cauchy stresses and Hencky strains, respectively. Using definitions (3), yield points represented on following figures form the intersections of the 3D yield surfaces in the principal stress space and the Rendulic plane, without any scaling.

Fig. 7.a,c shows plastic strain response envelopes for isotropic and closed die compaction of the sample for a constant stress increment magnitude $\Delta\sigma$. The value of $\Delta\sigma$ had to be tuned through a trial and error procedure and it is different for each initial loading path. It was chosen as small as possible, but large enough so that the incremental plastic strain response was significantly larger than numerical noise. As expected, the magnitude of plastic strain increment vectors increases with deviatoric stress such that, keeping a constant value of $\Delta\sigma$ for all the yield points, it is not possible to see all plastic response envelopes on the same graph. For this reason, plastic strain envelopes were normalised and represented in Fig. 7.b,d. Note that in the case of the closest yield point to the loadig point, underlined in Fig. 7.a, plastic strain increment vectors were too small to be detected. This is the reason why no normalised plastic strain envelope was plotted for this yield point in Fig. 7.b.

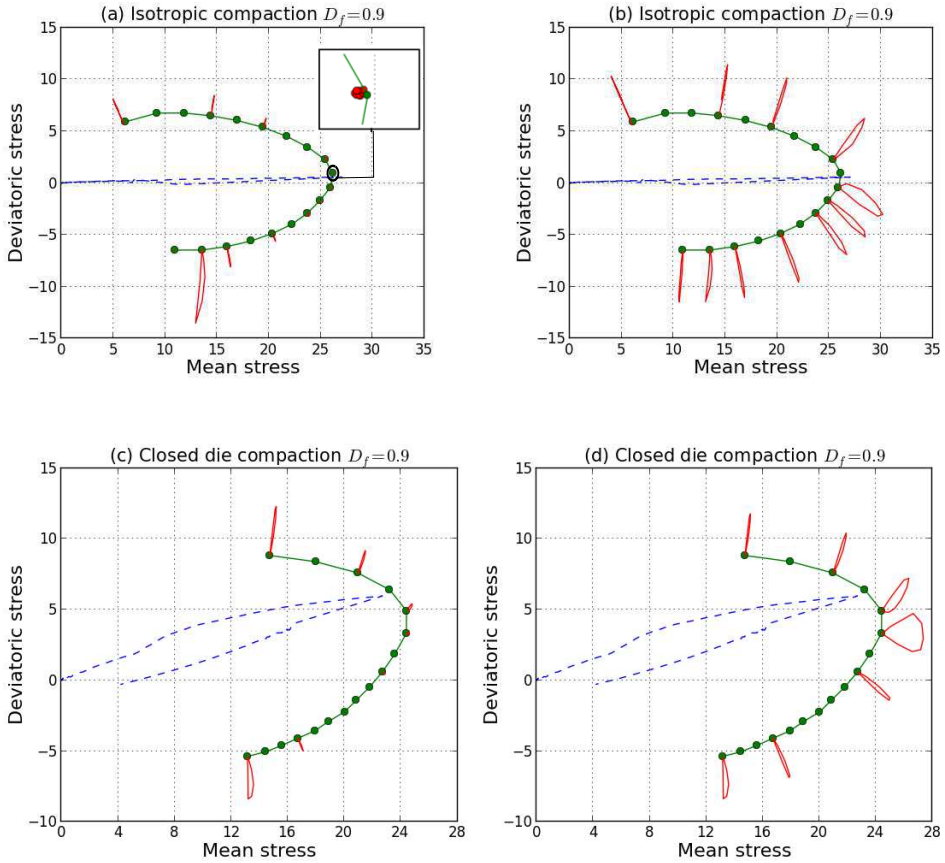

Figure 7: Plastic strain response envelopes for some points of the yield surface with final relative density $D = 0.9$. (a) and (b) Isotropic compaction. (c) and (d) Closed die compaction. In (b) and (d), plastic strain response envelopes have been normalised. The dotted line is the initial loading/unloading path.

Fig. 7.b,d show that most plastic strain increment vectors are close to line segments, and are approximately normal to the yield surface, suggesting the validity of an associated flow rule for such materials. This observation was made in the deviatoric stress (strain)/mean stress (strain) plane, and it is possible that 3D plastic strain response envelopes were planar surfaces, obviously different from line segments when plotted in the deviatoric plane, as it was observed for granular assemblies of rigid particles [14].

However, in the vicinity of the tip of the yield surfaces, plastic strain response envelopes can no more be assimilated to line segments. Such singular behaviour is confirmed by results presented in Figures 8 and 9. For low values of the final relative density D, plastic strain response envelopes suggest a highly non-associated behaviour close to the tips of closed-die-compaction yield surfaces, which becomes very striking at $D = 0.6$ (Fig.

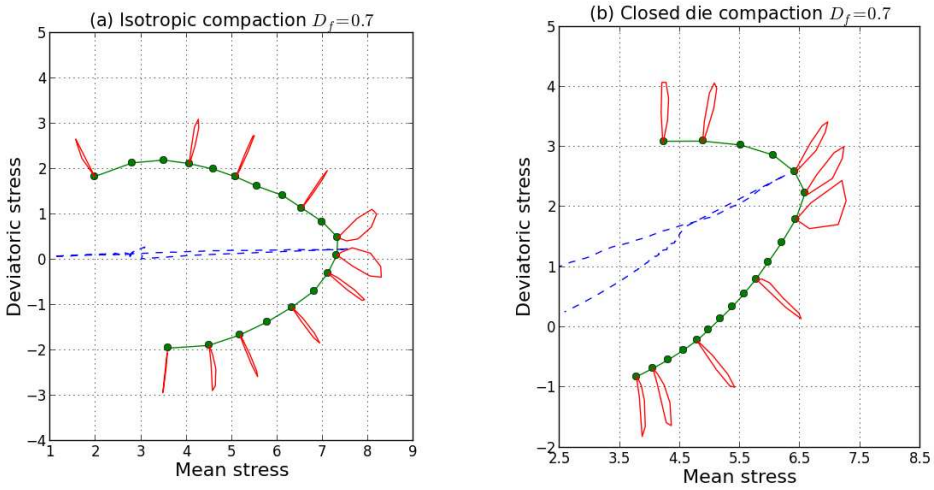

Figure 8: Normalized plastic strain response envelopes for some points of the yield surface with final relative density $D = 0.7$ for (a) isotropic and (b) closed die compaction. The dotted line is the initial loading/unloading path.

9.d). Results for $D = 0.9$ (Fig. 7.b,d) are closer to an associated-flow-rule material, which is probably the consequence of the sample becoming denser and thus, closer to the associated, Mises elastic-plastic constitutive model of the particles.

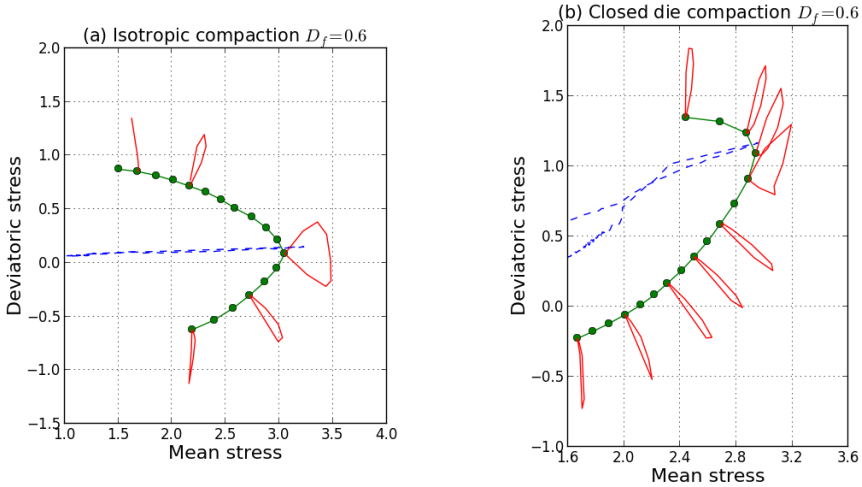

Figure 9: Normalized plastic strain response envelope for some points of the yield surface with final relative density $D = 0.6$ for (a) isotropic and (b) closed die compaction. The dotted line is the initial loading/unloading path.

[12] also showed using MPFEM simulations, that in a large deformation context, con-

tact surfaces between particles are created normal to the direction joining two particles, this direction remaining more or less constant during a monotonic loading such as isotropic or closed die compaction. As a result of this very special contact configuration, contact surfaces that increase in size during densification oppose an increasing resistance to normal stresses; and the particular loading that created the contact structure is precisely a loading for which contact surfaces essentially undergo normal loading. In the present case, this phenomenon results in plastic strain increment vectors being very small in magnitude.

The singular behaviour observed on plastic strain response envelopes could be related to the particular stress state corresponding to the loading point. Fleck et al. [5] obtained yield surfaces in the context of powder densification through a micromechanical modelling approach. In their results, loading points correspond to singular points of the yield surfaces, as a result of all the contacts experiencing purely normal loading, so that the direction of slip is undetermined. In the present case, it is not obvious that slip is the main mechanisms for plastic strains, but the increased resistance to normal loading of contacts might block plastic strains resulting from the stress state, leading to an increased significance of the role played by small stress increments in plastic deformation mechanisms.

4 CONCLUSIONS

This paper is concerned with the incremental plastic behaviour of ductile powder materials, i.e., granular materials with highly deformable elastic-plastic grains. Based on MPFEM simulations involving an assembly of meshed, deformable particles, the incremental plastic strain response of numerical samples to stress states on the plastic limit was studied. It was observed that such materials present a singular, highly non-associated behaviour in the vicinity of loading points, which is an original feature of the behaviour of ductile powders. In a small region of the principal stress state surrounding the loading points, the direction of the plastic strain increment vector shows a very significant dependency on the direction of the stress increment. This singular behaviour was attributed to the effect of contact surfaces resulting from grain deformation.

REFERENCES

[1] Brewin, P.R., Coube, O., Doremus, P. and Tweed, J.H. *Modelling of Powder Die Compaction*. Springer-Verlag London Limited. (2008) **374**.

[2] Drucker, D.C. and Prager, W. *Soil mechanics and plastic analysis or limit design*. Quarterly journal of mechanics and applied mathematics. (1952) **10**:157–175.

[3] Schneider, L.C.R. and Cocks, A. C. F. *Experimental in-vestigation of yied behaviour of metal powder compacts*. Powder Metallurgy. (2002) **345**:237–245.

[4] Pavier, E. and Dorémus, P. *Triaxial characterisation of iron powder behaviour*. Powder Metallurgy. (1999) **42**:345–352.

[5] Fleck, N. A., Kuhn, L. T. and McMeeking, R. M. *Yielding of metal powder bonded by isolated contacts*. Journal of the Mechanics and Physics of Solids. (1992) **40**:1139–1162.

[6] Martin, C. L. *Elasticity, fracture and yielding of cold compacted metal powders*. Journal of the Mechanics and Physics of Solids. (2004) **52**:1691–1717.

[7] Harthong, B., Jérier, J.-F., Richefeu, V., Chareyre, V., Dorémus, P., Imbault, D., Donzé, F.-V. *Contact impingement in packings of elastic-plastic spheres, application to powder compaction*. International Journal of Mechanical Sciences. (2012) **61**:32-43.

[8] Gethin, D. T., Lewis, R. W. and Ransing, R. S. *A discrete deformable element approach for the compaction of powder systems*. Modelling and Simulation in Materials Science and Engineering. (2003) **11**:101–114.

[9] Procopio, A. T. and Zavaliangos, A. *Simulation of multi-axial compaction of granular media from loose to high relative densities*. Journal of the Mechanics and Physics of Solids. (2005) **53**:1523–1551.

[10] Chen, Y., Imbault, D., Dorémus, P. *Numerical simula-tion of cold compaction of 3d granular packings*. Materials Science Forum. (2006) **534-536**:301–304.

[11] Schmidt, I., Kraft, T. and Wonisch, A. *Simulation of the material behavior of metal powder during compaction*. Proceedings of the Institution of Mechanical Engineers, Part E: Journal Process Mechanical Engineering. (2010) IMechE Vol. 224.

[12] Harthong, B., Imbault, D. and Dorémus, P. *The study of relations between loading history and yield surfaces in powder materials using discrete finite element simulations*. Journal of the Mechanics and Physics of Solids. (2012) **60**:784–801.

[13] Šmilauer, V., Catalano, E., Chareyre, B., Dorofeenko, S., Duriez, J., Gladky, A., Kozicki, J., Modenese, C., Scholtès, L., Sibille, L., Stránský, J., Thoeni, K., *Yade Documentation*. V. Šmilauer, ed., The Yade project, 1st ed. (2010). http://yade-dem.org/doc/.

[14] Calvetti F., Viggiani G. and Tamagnini C. *A numerical investigation of the incremental behavior of granular soils*. Italian Geotechnical Journal. (2003) **3**:11–29.

[15] Darve, F., and Nicot, F. *On flow rule in granular media: phenomenological and multiscale views (Part II)*. International Journal for Numerical and Analytical Methods in Geomechanics. (2005) **29**:1411–1432.